Evaluation of polarization effects of e^- collection Schottky CdTe Medipix3RX hybrid pixel detector

Vytautas Astromskas, Eva N. Gimenez, Annika Lohstroh and Nicola Tartoni, *Member, IEEE*

***Abstract*—This paper focuses on the evaluation of operational conditions such as temperature, exposure time and flux on the polarization of a Schottky electron collection CdTe detector. A Schottky e^- collection CdTe Medipix3RX hybrid pixel detector was developed as a part of the CALIPSO-HIZPAD2 EU project. The 128 x 128 pixel matrix and 0.75 mm thick CdTe sensor bump-bonded to Medipix3RX readout chips enabled the study of the polarization effects. Single and quad module Medipix3RX chips were used which had 128 x 128 and 256 x 256 pixel matrices, respectively. This study reports the sensor-level and pixel-level polarization effects of the detector obtained from a laboratory X-ray source. We report that the sensor-level polarization is highly dependent on temperature, flux and exposure time. Furthermore, the study of pixel-level polarization effects led to identification of a new type of pixel behaviour that is characterised by three distinct phases and, thus, named "tri-phase" (3-P) pixels. The 3-P pixels were the dominant cause of degradation of the flat-field image uniformity under high flux operation. A new method of identifying the optimum operational conditions that utilises a criterion related to the 3-P pixels is proposed. A generated optimum operational conditions chart under the new method is reported. The criterion is used for bias voltage reset depolarization of the detector. The method successfully represented the dependency of polarization on temperature, flux and exposure time and was reproducible for multiple sensors. Operating the detector under the 3-P pixel criterion resulted in the total efficiency not falling below 95%.**

***Index Terms*—Schottky CdTe, Semiconductor radiation detectors, Medipix, Polarization, Tri-phase pixels.**

I. Introduction

CADMIUM TELLURIDE's (CdTe) attractive properties such as high resistivity at room temperature and large linear attenuation coefficient make it a prospective semiconductor for room-temperature X- and gamma-ray radiation detectors. Recent improvements in crystal growth techniques allows the manufacturing of large area homogeneous crystals with electrical properties suitable for applications such as medical imaging, material science, synchrotron, and astrophysical applications [1, 2]. However, CdTe detectors, especially those with Schottky contacts, suffer from "polarization" effects that strongly affect the imaging performance of the detector, and in some cases cannot be suitably corrected by applying flat-field corrections [3].

Polarization causes a change in the detector's performance after biasing the sensor, and leads to a reduction in count rate over time and loss of charge collection efficiency. Polarization arises from trapping and de-trapping of ionized deep-level acceptors inside the crystal which affects the space-charge and electric field distribution [4]. The rate of polarization is influenced by operational conditions such as temperature, radiation flux, and duration of illumination [5]. Application of high bias voltages and operation at low temperatures can help to stabilize the detector's performance [4]. The most common method of depolarizing a detector is to reset the applied bias voltage which completely recovers the detector's performance [6]. However, to date no standardized procedure for depolarization has been established that identifies the optimum operational conditions the detector should be operated at in order to minimize the reset duration dead time in addition to minimizing the degradation of imaging quality. Hybrid small-pixel detectors can provide insight into the space-charge uniformity of the sensor. In hybrid detectors each pixel is individually connected to its electronic chain [7]. Previous studies of CdTe pixelated detectors have identified three types of pixel behaviour. Firstly, the majority of pixels follow the whole sensor's behaviour, i.e. exhibit a steady decrease of counts over time. Secondly, some pixels' counting performance remains stable. The third type of pixel behaviour shows a steady increase in counts over time. The increase in counts is usually observed in the pixels adjacent to a pixel without a contact, thus, the charge that would have been collected by a contactless pixel drifts to the adjacent ones [7].

In this study we present the evaluation of polarization effects on several Schottky e^- collection CdTe Medipix3RX pixelated detector systems, and the effect of operational conditions on the polarization. We report a new type of pixel behaviour that was used as a criterion for optimum bias voltage reset.

II. Methods

CdTe Schottky e^- collection sensors bump-bonded to Medipix3RX chips were used in this study in order to evaluate the polarization effects and determine the optimised operational conditions. CdTe sensors were manufactured by Acrorad [8]. Five single and five quad assemblies were manufactured as a part of the European CALIPSO-HIZPAD2 project. Single assemblies had 110 μm x 110 μm pixel pitch with a 128 x 128 pixel matrix, with dimensions of 14.2 mm x 14.2 mm x 0.75 mm. Quad assemblies had the same pixel pitch but 256 x 256 pixel matrix, with dimensions of 28.4 mm x 28.4 mm x 0.75 mm. The crystals were bump-bonded using InSn bump-bonds by Advacam [9]. The details on the Medipix3RX chip can be found in [10]. The MERLIN readout system, developed by the Diamond Light Source [11], was used for readout, control

V.Astromskas and A.Lohstroh are with University of Surrey, Guildford GU2 7XH, U.K (e-mail: v.astromskas@surrey.ac.uk; a.lohstroh@surrey.ac.uk)

E.N.Gimenez and N.Tartoni are with Diamond Light Source Ltd., Didcot, Oxfordshire OX11 0DE, U.K (e-mail: nicola.tartoni@diamond.ac.uk; eva.gimenez-navarro@diamond.ac.uk)

of bias voltage reset, and monitoring the temperature of the detector [12]. The results presented in this paper were obtained using the single pixel counting mode of the Medipix3RX chip.

All of the experiments were performed using a Molybdenum target laboratory X-ray tube with a maximum voltage of 50 kVp and a maximum current of 50 mA. A direct X-ray beam was used to uniformly illuminate the detector placed approximately 70 cm from the X-ray tube. The Medipix3RX chip was inside a 2 mm thick Al casing. The Al casing had a window which only revealed the CdTe crystal. The incoming 25 keV X-rays were 100% absorbed by the CdTe crystal [2], thus protecting the metal bonding between the ASIC and the crystal. The chip itself had a 4 μm thick Al layer deposited on it. The circuitry in the periphery of the CdTe crystal is digital, i.e. any radiation damage on the circuitry would register as digital errors due to the fact that the impact of radiation would be seen as a change of the timing properties of the circuit. This is not the case for the results presented in this paper. The detectors were tested under several temperatures and radiation fluxes. The thermal stability of the detector was ensured using a water chiller and a copper plate at the back of the detector assembly. The temperatures for measurements ranged from 10 °C to 24 °C. The fluxes of the direct X-ray beam at the position of the detector ranged from 9 kcps per pixel to 300 kcps per pixel. The relationship between the current of the X-ray tube and the registered counts per pixel per second is displayed in figure 1. The applied bias voltage was set to -500 V for all measurements.

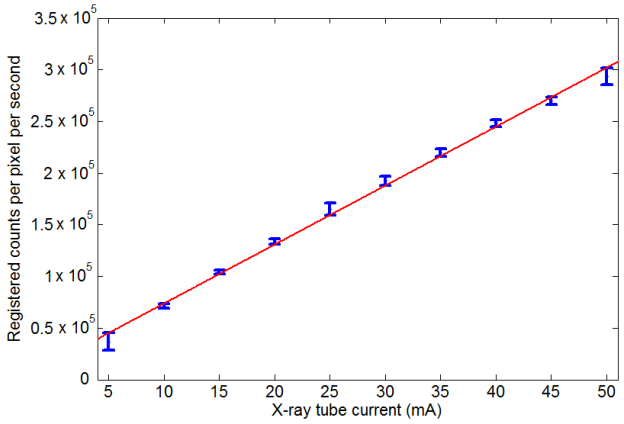

Fig. 1. The linearity of the registered counts per pixel per second with respect to the current of the X-ray tube. The errors were extracted from the linear fit.

III. Results and Discussion

A. Sensor-level polarization effects

Figures 2 and 3 show the reduction of mean counts per frame over time with respect to temperature and flux respectively. Each point in these figures was obtained by summing the counts of each pixel of a sensor in a frame and normalizing to the first frame's count value. The detector was exposed to radiation for 90 minutes without a bias voltage reset applied. The acquisition time of each frame (i.e. frame rate) in figure 2 was 300 ms. In figure 3 the frame rate was 30 s, 300 ms and 100 ms for 100 cps, 9 kcps and 24 kcps per pixel, respectively. Observations from single and quad module detectors agree with previously published results, i.e. cooling the detector reduces the rate of efficiency degradation [4]. The degradation with higher temperature arises as the number of thermally generated charge carriers increases. Also, the results show that the polarization is highly dependent on flux and the duration of radiation illumination. The slopes of time dependencies of normalized number of counts in each sensor of a quad module detector slightly differ depending on the defects. No pixels were excluded in the analysis. Radiation flux increases the ionization rate of electron-hole pairs inside the semiconductor. This results in an increased number of free charge carriers which can be trapped by the defects and impurities causing polarization to occur sooner.

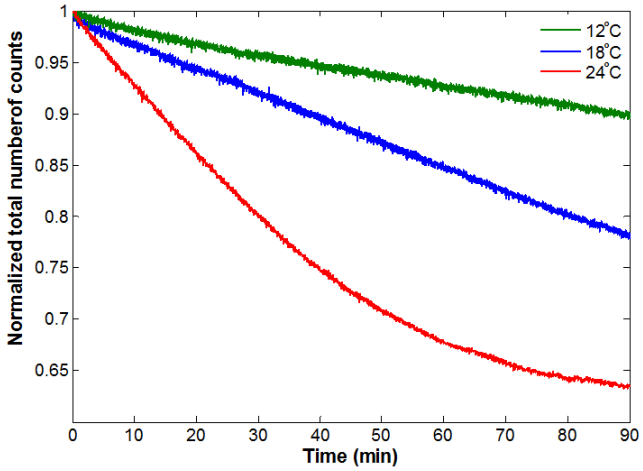

Fig. 2. Polarization dependency over time for different temperatures. The detector was illuminated under the same conditions of 9 kcps per pixel flux from the Molybdenum target X-ray tube.

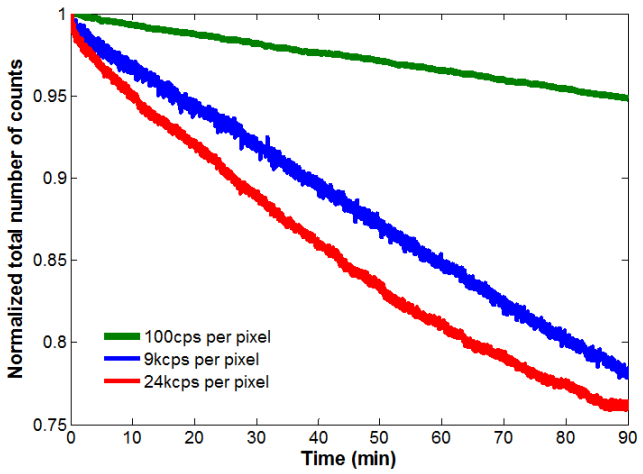

Fig. 3. Polarization dependency over time for different photon fluxes. The detector was cooled to 18 °C for all measurements.

The degradation of the sensor's performance arising from polarization is typically identified as a loss of counts, appearance of dislocation lines, and reduction in the total uniformity of response [4]. Figure 4 shows four flat-field images of a sensor obtained under different conditions. The detector was

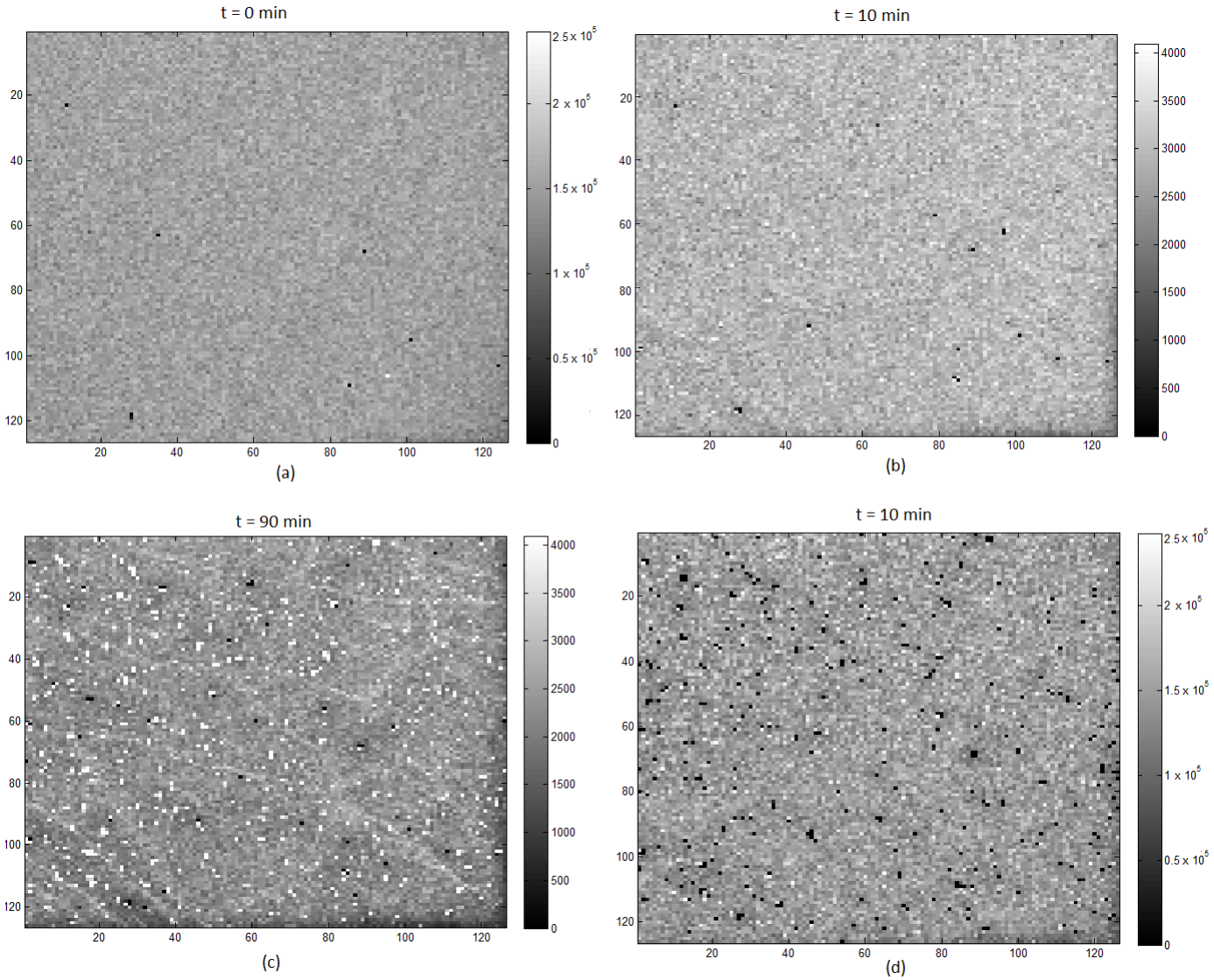

Fig. 4. Flat-field images of a quadrant of a quad detector. The detector was cooled to 18 °C. Flat-field image of the first frame of exposure (a). Flat-field after a 10 minute exposure at 9 kcps per pixel flux (b). Flat-field after 90 minute exposure at 9 kcps per pixel flux (c). Flat-field image after a 10 minute exposure at 300 kcps per pixel (d). The 24-bit counter was used to obtain flat field images (a) and (d). The 12-bit counter was used to obtain flat field images (b) and (c).

operated at 18 °C temperature. The frame rate was 500 ms. Fig.4(a) shows an initial frame of the illumination under 300 kcps per pixel flux. Fig.4(b) displays the degradation of the sensor after a 10 minutes of 9 kcps radiation flux. Fig.4(c) displays the degradation of the sensor after a 90 minute illumination of 9 kcps flux of X-rays. Fig.4(d) shows the degradation of the sensor after a 10 minute exposure of 300 kcps flux of X-rays. The difference in the total number of counts in the frame differs due to one (12 bit) or two (24 bit) counters being enabled during the acquisition. Fig.4(a) and Fig.4(d) used a 24 bit counter, while Fig.4(b) and Fig.4(c) used the 12 bit counter.

Figure 4 shows that the dominating polarization effect of the sensor, i.e. having the greatest impact on the uniformity of sensor's response, differs with flux. As shown in Fig.4(c), the dominating defects under low flux and long exposure are loss of total counts and dislocation lines, and saturated pixels which appear in white. With the 12 bit counter, a saturated pixel recorded a maximum of 4095 counts per frame. Under the high flux operation, as shown in Fig.4(d), the dominating effect is the tri-phase (3-P) pixels which count zero. The 3-P pixel's behaviour is discussed in section III-B. For comparison, Fig.4(b) and Fig.4(d) show the difference in degradation after 10 minute exposure but for 9 kcps and 300 kcps flux respectively. It is worth noting that depolarizing the detector using bias voltage reset restored the response of all the pixels to the original state as shown in Fig.4(a) for all detectors including the 3-P pixels which is discussed later in section III-C.

The uniformity of response was evaluated using flat-field coefficient histograms. The flat-field coefficient values are obtained by dividing each pixel's count value by the mean

count value of the whole sensor. This resulted in a histogram of flat-field coefficients as shown in figure 5. The flat-field coefficient values in Fig.5(a) were obtained from the flat-field image of Fig.4(a), while the Fig.5(b) histogram coefficient values were obtained from the flat-field of Fig.4(d). Due to the polarization effects, the total uniformity of the detector's response to radiation decreases over time as the width of the histogram increased. The skew of the distribution towards higher flat-field coefficient values in both histograms arises from the reduction of efficiency of the detector due to polarization. The reduction of the registered counts requires a flat-field coefficient value greater than 1 in order to correct the pixel's counts to the mean counts of the sensor. A Gaussian distribution of the flat-field coefficients is expected in the first frame as a Gaussian pixel-threshold calibration was performed on all the sensors around the noise edge. The skew in the Fig.5(a) shows that the polarization effect is already observed in the first frame.

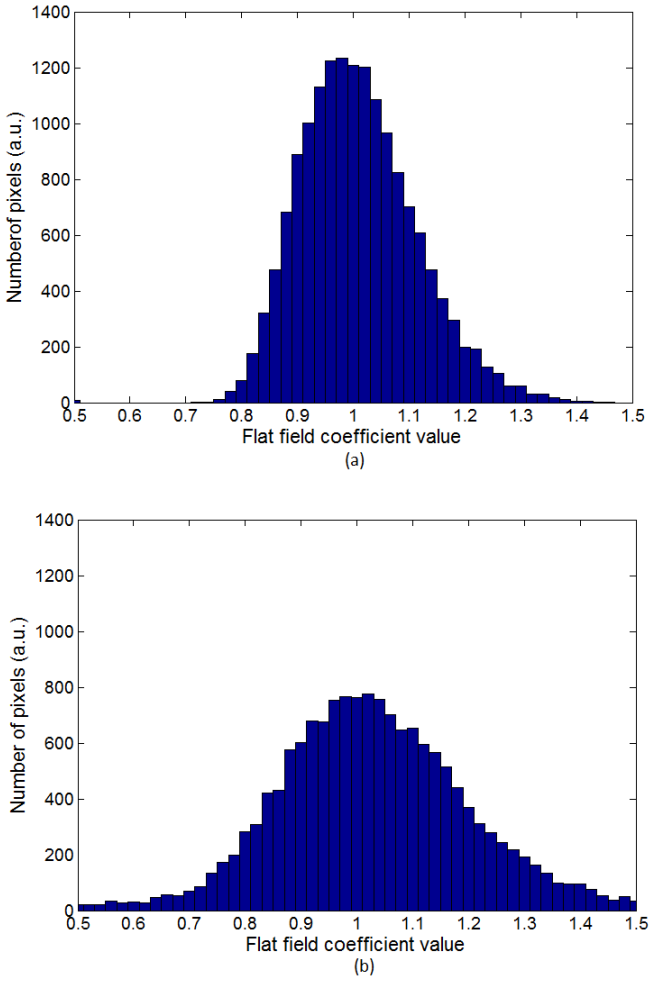

Fig. 5. Flat-field coefficient histogram showing the uniformity of pixel response on the sensor. The detector was operated under 18 °C temperature and 300 kcps count rate. First frame's uniformity is represented in (a). Detector uniformity after a 10 minute exposure is shown in (b).

B. Pixel-level polarization effects

All three previously reported types of pixel behaviours (mentioned in section I) were observed in our detectors. Furthermore, a fourth type of pixel behaviour was observed in our single and quad assemblies that dominated the degradation of the flat-field images under high flux which has not been reported before. The tri-phase pixel behaviour is shown in figure 6. The first phase was identified as a steady increase of counts. In the second phase, there is a more rapid increase of counts up to a certain value of counts. The maximum number of counts slightly varied for every pixel as seen in figure 7. During the third phase, the total number of counts decreased at different rates but always reached zero within 30 seconds, which left the pixel not counting until the bias voltage reset was applied. Figure 7 shows the counts as a function of time for two example pixels in each quadrant of a quad module. The pixels were neither adjacent to each other nor near underperforming pixels. These pixels were identified as the zero counts pixels at the end of a 10 minute cycle as seen in Fig.4(d). The total number of this type of pixel increased over time and they all showed a similar behaviour to that shown in figure 7. Furthermore, these pixels were consistently observed in each of the sensors tested in the first and third quad assemblies (i.e. 8 different sensors), and exhibited the same behaviour over multiple cycles as shown in figure 9. The second and fourth quad assemblies were not tested as they were inoperable due to faults during the detector's assembly.

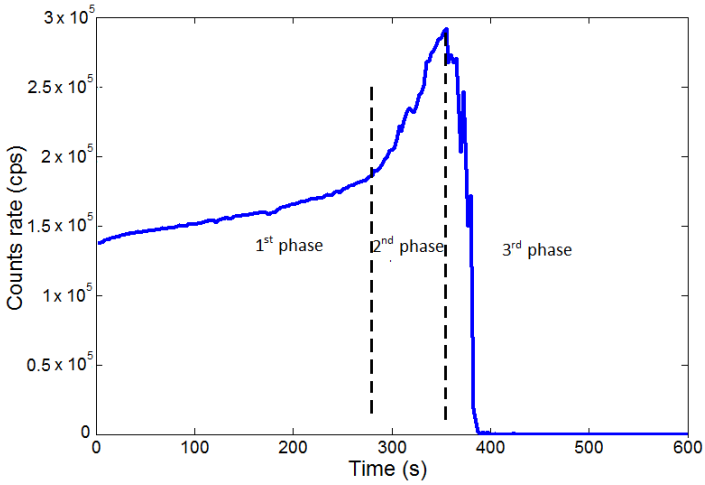

Fig. 6. A typical tri-phase pixel behaviour with the three main phases identified.

The physics behind the 3-P pixel's behaviour is not currently understood and has not yet been investigated in sufficient detail. From a preliminary evaluation of the performance of the 3-P pixels and their neighbours it can be deduced that the underlying mechanisms are limited to the 3-P pixel as in most cases the nearby pixels are not affected. This suggests that the effect is near the surface of the crystal. If the origin was located deep in the crystal, diffusion of the generated charge would cause it to drift to the electrodes of multiple pixels.

C. Criterion for bias voltage reset

There is not a standard criterion under which the bias voltage should be reset that specifies how often it may occur and for how long the "off-time" should last. The identification

of pixels that behave as described in section III-B provide a criterion for bias voltage reset, since the 3-P pixels dominated the sensor's degradation of uniformity under high flux.

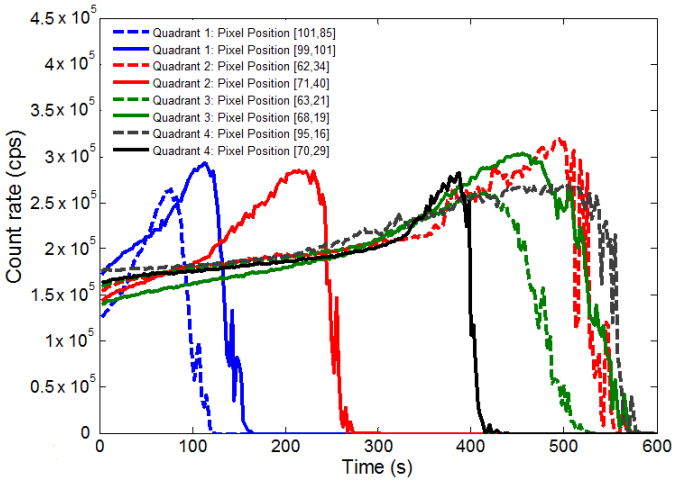

Fig. 7. 3-P pixels' behaviour from each of the quadrants from a quad assembly.

Figure 8 shows the increase of the total number of 3-P pixels as a function of time under different count rates. The detector was cooled to 10 °C and the data was collected for 10 minutes with a 500 ms frame rate and no bias voltage reset applied. Three features can be observed in this figure. First, there is a baseline, i.e. the sensor has some pixels that constantly count zero. These are the inactive pixels due to either contact issues or being masked, i.e. the electronics behind it were deactivated. The total number of inactive pixels is different for each sensor. Secondly, there is a stable plateau where the total number of 3-P pixels does not change or fluctuate by ± 1. The plateau fundamentally corresponds to the duration the detector is stable with respect to 3-P pixels. The duration of the plateau region was dependent on flux and temperature. Thirdly, a steady increase of the total number of 3-P pixels. The rate of increase was dependent on both flux and temperature. These features suggest a criterion which quantifies the time at which the plateau region ends.

In order to determine the criterion for each sensor a different baseline definition is required. The baseline is determined by the total number of inactive pixels in the first frame and adding an offset of a standard deviation of the inactive pixels. The addition of this offset is required in order to ignore the minor fluctuations in the number of 3-P pixels as shown in the 40 kcps per pixel dataset in figure 8. This way the criterion takes into account the whole sensor's behaviour. The criterion identifies the instance in time where the total number of 3-P pixels is higher than the defined baseline, i.e. the end of the stable plateau. The extracted time value was used as the bias voltage reset time. This process was repeated for each of the fluxes and the temperatures tested. The generated criteria produced an optimum operational conditions (OOC) chart as seen in figure 10. The figure shows the time at which the bias voltage should be reset for different operating temperatures and incident average flux, and should be read as a chart. The X-axis denotes the time when the detector should be depolarized according to the criterion. The Y-axis displays the flux under which the detector was illuminated from the X-ray tube. The corresponding registered number of counts for each of the X-ray tube currents is shown in figure 1. The criterion ensures that flat-field image quality is kept at the best (optimal) state as the moment in time when the 3-P pixels start appearing in the flat-field image, the detector is re-set. As the 3-P pixel behaviour cannot be compensated for by flat-field corrections, we consider the optimum condition to re-set the detector as soon as the 3-P pixels begin to increase in number, in order to minimise their effect on the corrected image quality. The OOC charts are reproducible for all sensors despite their different polarization responses.

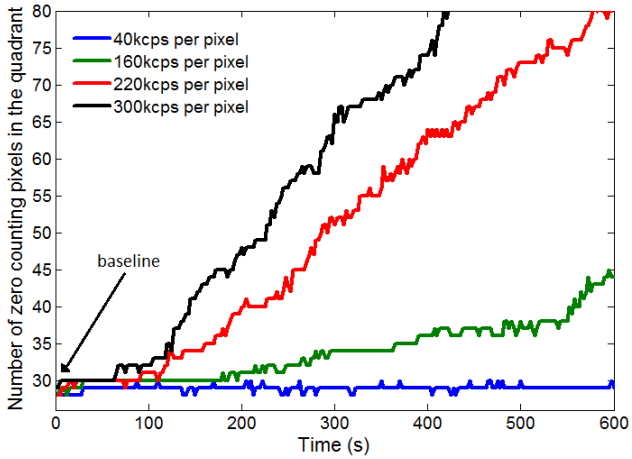

Fig. 8. Increase of the total number of 3-P pixels in the sensor over time. The criterion is met when the total number of 3-P pixels is above the baseline value.

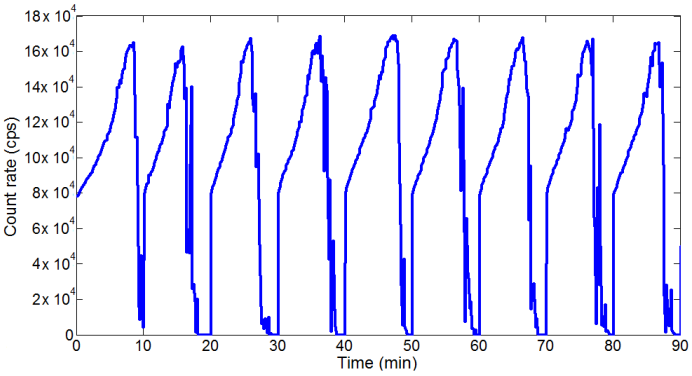

Fig. 9. A single 3-P pixel's reproducible behaviour over nine 10 minute cycles.

An empirical approach to fit the data shown in figure 10 with double exponential was chosen as a single exponential did not fit the data correctly. The double exponential could suggest that the polarization has a fast and a slow component. The extracted time decay constants were in the range of 0.03 ± 0.02 s^{-1} and 0.002 ± 0.001 s^{-1} for the first and second exponential respectively, within the limitations of the precision of the individual fits. It was not possible to identify any further systematic dependency on the operating conditions

with confidence. As shown in figure 10, the colder the detector the longer it can operate before the criterion is met, which agrees with previously published data [5]. In addition, the total efficiency of the detector did not degrade below 95% when applying the extracted depolarization time from the criterion.

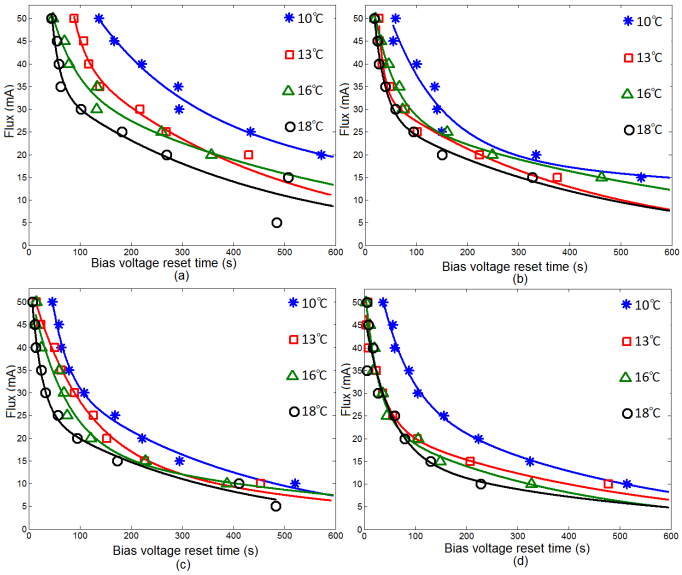

Fig. 10. Optimum Operational Conditions (OOC) charts for each of the sensor of a quad assembly: for the 1st quadrant (a), 2nd quadrant (b), 3rd quadrant (c) and 4th quadrant (d). Each point of each line represents the time instance, where the criterion is met, and its dependence on flux and temperature. The corresponding registered counts per pixel per second to the flux are shown in Fig.1.

D. Bias Voltage reset duration

A common way of depolarizing the detector is to reset the applied bias voltage on the detector. The applied bias voltage is ramped down from -500 V to 0 V over a period of 5 s in all measurements. The longer the bias voltage remains switched off following the end of the ramping time the more trapped charge is released. This was observed by investigating the 3-P pixels' behaviour when the bias voltage was being reset. While the bias voltage was ramping down towards zero volts, the pixel was activated and counted more than the nearby pixels, which suggested that the trapped charge was being released.

We have investigated the effect of the duration of the bias voltage remaining switched off. Figure 11 shows the loss of the total number of counts for each of the sensors of the quad assembly with different durations of bias voltage being switched off.

The tested "off time" durations i.e. after the bias voltage reached 0 V, were 1, 10, 15 and 20 seconds. The detector was operated under 300 kcps per pixel flux and cooled to 18 °C. The frame rate was 500 ms. Note the mean pixel value of the final frame of each cycle decreased when the bias reset time was too short. This effect is visible in the Fig.11(a) and Fig.11(b) plots. This arises from the sensor not fully depolarizing, hence, taking less time for polarization to build up. However, Fig.11(c) and Fig.11(d) show that the bias reset duration was long enough to keep the detector stable in between the cycles. The behaviour of the fourth quadrant followed the same trend as the other three but it has been excluded from the figure 11 as it had noisy pixels which disrupted the plot. Additionally, a small overshoot is observed after the bias reset was applied. The overshoot is caused by the sensor needing some time to stabilise. The overshoot is of approximately 2% of the total number of counts and lasts less than three seconds. The black line is set to one for a clear display of the overshoots.

The duration of the bias voltage to be switched off was dependent on the degradation of performance of the detector and the operational conditions. For low flux measurements it has been observed that a shorter "off time" was sufficient to completely depolarize the detector and keep it stable over multiple cycles.

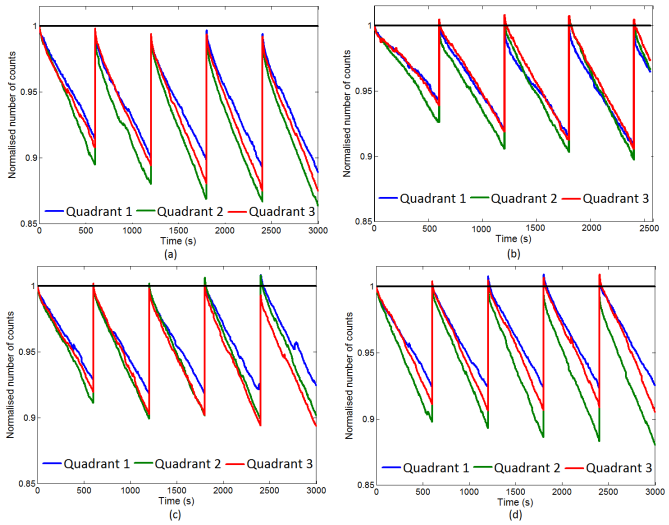

Fig. 11. Mean values for each frame during several refreshing bias cycles for three quadrants of a quad assembly and for different bias refresh times: with a 1 s refresh time (a), 10 s (b), 15 s (c) and 20 s (d). The black line is set to one for a clear display of the overshoots.

IV. Conclusion

A Schottky e^- collection CdTe sensor bump-bonded to a Medipix3RX chip was used to evaluate the effects of operational conditions onto polarization. The results showed that in single and quad assemblies the polarization is highly dependent on temperature, flux and radiation exposure time. These operational conditions must be taken into consideration when operating the system. Furthermore, an identification of a new type of pixel behaviour led to definition of 3-P pixels. The 3-P pixels cannot be easily corrected using flat-field correction as they exhibit non-linear behaviour over time. The underlying mechanism behind the 3-P pixels should be fully investigated in future.

The 3-P pixels were used as a criterion in order to determine the optimal time to apply high voltage reset for stabilising the detector's performance using an Optimal Operational Conditions (OOC) chart. The 3-P pixels were the dominant flat-field defect under high flux conditions. Under the proposed method the applied bias voltage is reset as soon as the 3-P pixels appear in the flat-field image. This eliminates any 3-P pixels and only linearly degrading pixels remain which can

be easily corrected using flat-field corrections. When applying the optimal depolarization time the detector's efficiency did not reduce below 95%. The proposed method is performed on the whole sensor and was found to be reproducible for multiple sensors. The generated OOC chart would assist users of the detector in maintaining the best flat-field quality as it allows extracting the optimal depolarization time for a range of operational conditions.

ACKNOWLEDGEMENT

This project is funded by SEPnet and the HIZPAD2 Joint Research Activity, part of the European funded CALIPSO project, grant agreement 312284. The authors would like to thank Ian Horswell, David Omar and Richard Plackett at the Diamond Light Source for assistance with the operation of the MERLIN system.

REFERENCES

[1] H. Shiraki, M. Funaki, Y. Ando, S. Kominami, K. Amemiya, and R. Ohno, "Improvement of the Productivity in the THM Growth of CdTe Single Crystal as Nuclear Radiation Detector," *IEEE Transactions on Nuclear Science*, vol. 57, pp. 395–399, Feb. 2010.

[2] S. D. Sordo, L. Abbene, E. Caroli, A. M. Mancini, A. Zappettini, and P. Ubertini, "Progress in the Development of CdTe and CdZnTe Semiconductor Radiation Detectors for Astrophysical and Medical Applications," *Sensors (Basel, Switzerland)*, vol. 9, pp. 3491–3526, May 2009.

[3] R. Aamir, S. P. Lansley, R. Zainon, M. Fiederle, A. Fauler, D. Greiffenberg, P. H. Butler, and A. P. H. Butler, "Pixel sensitivity variations in a CdTe-Medipix2 detector using poly-energetic x-rays," *Journal of Instrumentation*, vol. 6, p. C01059, Jan. 2011.

[4] M. Niraula, A. Nakamura, T. Aoki, Y. Tomita, and Y. Hatanaka, "Stability issues of high-energy resolution diode type CdTe nuclear radiation detectors in a long-term operation," *Nuclear Instruments and Methods in Physics Research Section A: Accelerators, Spectrometers, Detectors and Associated Equipment*, vol. 491, pp. 168–175, Sept. 2002.

[5] I. Farella, G. Montagna, A. Mancini, and A. Cola, "Study on instability phenomena in CdTe diode-like detectors," in *IEEE Nuclear Science Symposium Conference Record, 2008. NSS '08*, pp. 154–161, Oct. 2008.

[6] R. O. Bell, G. Entine, and H. B. Serreze, "Time-dependent polarization of CdTe gamma-ray detectors," *Nuclear Instruments and Methods*, vol. 117, pp. 267–271, May 1974.

[7] C. Buton, A. Dawiec, J. Graber-Bolis, K. Arnaud, J. F. Brar, N. Blanc, N. Boudet, J. C. Clmens, F. Debarbieux, P. Delpierre, B. Dinkespiler, T. Gastaldi, S. Hustache, C. Morel, P. Pangaud, H. Perez-Ponce, and E. Vigeolas, "Comparison of three types of XPAD3.2/CdTe single chip hybrids for hard X-ray applications in material science and biomedical imaging," *Nuclear Instruments and Methods in Physics Research Section A: Accelerators, Spectrometers, Detectors and Associated Equipment*, vol. 758, pp. 44–56, Sept. 2014.

[8] "Acrorad - CdTeŁ." http://www.acrorad.co.jp/us/. Accessed: 2015-06-25.

[9] "Advacam - Imaging the unseen - Home." http://www.advacam.com/en/. Accessed: 2015-06-25.

[10] R. Ballabriga, J. Alozy, G. Blaj, M. Campbell, M. Fiederle, E. Frojdh, E. H. M. Heijne, X. Llopart, M. Pichotka, S. Procz, L. Tlustos, and W. Wong, "The Medipix3rx: a high resolution, zero dead-time pixel detector readout chip allowing spectroscopic imaging," *Journal of Instrumentation*, vol. 8, p. C02016, Feb. 2013.

[11] "Diamond Light Source." http://www.diamond.ac.uk/Home.html. Accessed: 2015-06-25.

[12] R. Plackett, I. Horswell, E. N. Gimenez, J. Marchal, D. Omar, and N. Tartoni, "Merlin: a fast versatile readout system for Medipix3," *Journal of Instrumentation*, vol. 8, p. C01038, Jan. 2013.